High-density speckle contrast optical tomography (SCOT) for three dimensional tomographic imaging of the small animal brain

Tanja Dragojevi, Hari M. Varma, Joseph L. Hollmann, Claudia P. Valdes, Joseph P. Culver, Carles Justicia, Turgut Durduran

PII: S1053-8119(17)30291-4
DOI: http://dx.doi.org/10.1016/j.neuroimage.2017.04.003
Reference: YNIMG13944

To appear in: *NeuroImage*

Received date: 9 December 2016
Revised date: 27 February 2017
Accepted date: 1 April 2017

Cite this article as: Tanja Dragojevi, Hari M. Varma, Joseph L. Hollmann, Claudia P. Valdes, Joseph P. Culver, Carles Justicia and Turgut Durduran, High-density speckle contrast optical tomography (SCOT) for three dimensiona tomographic imaging of the small animal brain, *NeuroImage* http://dx.doi.org/10.1016/j.neuroimage.2017.04.003

High-density speckle contrast optical tomography (SCOT) for three dimensional tomographic imaging of the small animal brain

Tanja Dragojević[1,*], Hari M. Varma[1,*], Joseph L. Hollmann[1*], Claudia P. Valdes[1], Joseph P. Culver[2,3], Carles Justicia[4,5], Turgut Durduran[1,6]

[1] *ICFO-Institut de Ciències Fotòniques, The Barcelona Institute of Science and Technology, 08860 Castelldefels (Barcelona), Spain*
[2] *Department of Radiology, Washington University School of Medicine,St. Louis, MO 63110, USA*
[3] *Department of Physics, Washington University, St. Louis, MO 63130, USA*
[4] *Department of Brain Ischemia and Neurodegeneration, Insitut d'Investigacions Biomèdiques de Barcelona (IIBB), Consejo Superior de Investigaciones Científicas (CSIC), Barcelona, Spain*
[5] *Àrea de Neurociències, Institut d'Investigacions Biomèdiques August Pi i Sunyer (IDIBAPS), Barcelona, Spain*
[6] *Institució Catalana de Recerca i Estudis Avançats (ICREA), 08015 Barcelona, Spain*
[*] *These authors contributed equally.*

Abstract

High-density speckle contrast optical tomography (SCOT) utilizing tens of thousands of source-detector pairs, was developed for *in vivo* imaging of blood flow in small animals. The reduction in cerebral blood flow (CBF) due to local ischemic stroke in a mouse brain was transcanially imaged and reconstructed in three dimensions. The reconstructed volume was then compared with corresponding magnetic resonance images demonstrating that the volume of reduced CBF agrees with the infarct zone at twenty-four hours.

Keywords:

OCIS codes: (170.3880) Medical and biological imaging; (110.3010) Image reconstruction techniques; (110.6150) Speckle imaging;

1. Introduction

Cerebral blood flow (CBF) plays a crucial role in supplying the brain tissue with oxygen and removing the by-products of metabolism such as carbon dioxide [1]. In particular, microvascular CBF is locally controlled in order to maintain healthy brain functions. Alterations of the regulation of CBF due to conditions like ischemic stroke have severe consequences, thus, it is critical to reliably and frequently measure microvascular CBF.

To date, several techniques have been developed and utilized with varying levels of success. For example, perfusion computed tomography (PCT) [2], diffusion and perfusion weighted magnetic resonance imaging (MRI) [3] are often employed for the diagnosis of ischemic stroke for determining the infarct and penumbra volumes [4]. Although it is possible to image microvascular cerebral blood flow with mentioned techniques (and others), they have limitations due to non-portability or the usage of radio-pharmaceutics. The need for non-invasive and bedside monitoring is pressing [5].

Near-infrared diffuse optical spectroscopy (NIRS-DOS) is a promising technology because it is non-invasive and portable. Furthermore, it is suitable for longitudinal, bedside monitoring and imaging [6]. Traditional NIRS-DOS measures microvascular blood oxygen saturation and volume, CBF can be estimated using specific challenges or contrast agents. NIRS-DOS can also be employed in a tomographic manner, i.e. diffuse optical tomography (DOT) [6], by utilizing a multitude of sources and detectors with an inversion algorithm to reconstruct the underlying tissue properties in three dimensions. DOT is able to achieve three dimensional reconstruction of cere-

bral hemodynamics in small animals too [7, 8], where some designs have used a CCD camera for detection [9, 10]. Furthermore, it has been shown that with high-density DOT, i.e. utilizing a dense array of source-detector pairs covering a wide range of source-detector separations, is possible to achieve better resolution and localization accuracy compared to sparse topography arrays [11].

Optical techniques that quantify the intensity fluctuations of diffuse speckles estimate the motion of red blood cells and thus directly measure microvascular blood flow. For small animal imaging, minimally invasive techniques for monitoring CBF include laser speckle imaging (LSI) [12, 13, 14] and laser Doppler flowmetry (LDF) [15]. LDF measures the Doppler shift in frequency of the re-emitted light from the sample. Furthermore, LDF, in general, measures relative blood flow, not absolute, and is limited to superficial layer of tissue (< 1 mm) [16]. The LSI uses a coherent laser source and an array detector (CCD/CMOS) to measure blood flow. A statistical quantity called speckle contrast is computed for a given exposure time and a model is utilized to extract CBF. By employing multiple exposure times [17] absolute and longitudinal measurements are possible. Although this technique is quite promising, there are several disadvantages. LSI with a uniform (or near-uniform) illumination scheme constrains the measurement of cerebral hemodynamics to $<$ 1mm from the tissue surface. LDF and LSI are both ineffective for resolving CBF in three dimensions.

On the other hand, diffuse correlation spectroscopy (DCS) [6, 18, 19], is based on photon diffusion in deep tissues. This technique gives a direct measurement of rCBF by measuring the movement of the scattering particles

(red blood cells) with sources and detectors separated from few millimeters to several centimeters. DCS and its tomographic equivalent diffuse correlation tomography (DCT) have been extensively validated and employed for monitoring rCBF in small animal models [7, 20, 21, 22]. The main drawback of DCT for small animal imaging is that high-density approaches would require many detection channels that are prohibitively expensive, the signal-to-noise ratio due to the low count rates and the dynamic range is limited.

Recently, we [23, 24] and others [25, 26, 27, 28, 29] have introduced a relatively inexpensive alternative to DCS, a speckle contrast based deep tissue spectroscopic method called speckle contrast optical spectroscopy (SCOS) [23]. SCOS merges the deep tissue flow measurement capabilities of DCS and the relatively inexpensive detectors with high frame rates that are used in LSI. This technique was demonstrated in tissue mimicking phantoms and *in vivo* experiments for quantitative measurements of blood flow with SCOS, [23, 26, 27]. We [24] and others [28] have introduced a tomographic expansion, to which we refer as speckle contrast optical tomography (SCOT), that allows three dimensional tomography of blood flow. However, these publications were mostly utilizing phantoms. In this paper we demonstrate SCOT for *in vivo* cerebral blood flow measurement in mice.

Here, we introduce a high-density SCOT setup developed for the minimally invasive measurement of cerebral blood flow in small animals. Thousands of detectors are used to reconstruct volumetric change of blood flow after the induction of a local ischemic stroke. We present the quality of the raw data and the high information content in the high-density data set. Three dimensional tomographic and quantitative images of cerebral blood

flow obtained with SCOT are compared to the infarct volume observed by anatomical magnetic resonance imaging (MRI) at 24 hours.

2. Methods and materials

2.1. Setup for speckle contrast optical tomography

The SCOT system, shown in Fig. 1, consists of a scanning arm equipped with a temperature controlled, continuous wave, 785 nm laser diode (Thorlabs, Germany) and optical elements: an aspheric lens used to focus the laser beam to an anamorphic prism pair to get a spatially symmetric beam which is then passed through an aperture and a convex lens to a pair of galvo-mirrors (Nutfield, USA, QS-7) which take the beam to the sample. The focal length of the convex lens was selected so that the beam is focused to the sample with the spot diameter of 0.05 cm. The number of sources used for analysis varied slightly from animal to animal due to the physical restrictions (dental cement, etc.), but, on average, 20 source positions were used with the scanning geometry shown in Fig. 2(a).

The diffuse light from the sample produces speckles which are imaged from the top with a 12 bit, monochrome scientific CCD camera (Basler, Germany, scA640-120fm, quantum efficiency 42.22% at 785 nm) with an exposure time of 5 ms and a horizontal field of view of 1 cm by 1.2 cm. A green LED was positioned below the camera for evaluation of animal preparation. Each pixel over the image corresponds to a specific distance from the source. In total, 1000 images were acquired at 50 fps per scanning position (20 s) to ensure a good signal-to-noise ratio (SNR).

[Figure 1 about here.]

[Figure 2 about here.]

2.2. Magnetic resonance image acquisition

A 7T MRI magnet (Bruker BioSpin, Germany) was used to collect T2 weighted images using multi-slice multi-echo (MSME) protocol with a field-of-view (FOV) of 2 cm by 2 cm, with a coronal and axial slice orientation. Eighteen slices were acquired with a slice thickness of 0.5 mm and a pixel resolution of 0.078 mm^2/pixel. Sixteen echoes were collected with an effective echo time (TE) of 11 ms to 176 ms, in steps of 11 ms, and a repetition time (TR) of 4764.3 ms.

We note here that we have used anatomical MRI images which were acquired 24 hours after the optical image. The delay was required because, during the acute phase of the lesion, MRI anatomical sequences are not able to detect the limits of an affected region [30]. Diffusion and perfusion weighted images are more appropriate at early hours but are limited to a single slice.

2.3. Animals and stroke model

The animal studies were conducted with the approval of the ethical committee of the University of Barcelona, the local authorities, and according to the Spanish and European regulations. Adult male C57/BL6 mice (age 4-6 months and weight 25-30g) were anesthetized with 4% isoflurane (O_2:N_2O (30:70)). The mice were moved to a stereotaxic frame and the anesthesia was reduced and maintained at 2% isoflurane. The scalp was removed and a Teflon ring was attached to the skull with a dental cement. The ring was filled with mineral oil (Sigma Aldrich, USA) to prevent the skull from drying

out [31]. Throughout the experiment, the body temperature was maintained around 37 ± 0.5^{o}C with a heating blanket.

A focal ischemia was induced by photothrombosis [32] in the right hemisphere of the brain. This was accomplished by intraperiotoneally injecting Rose Bengal dye (0.1ml of a 10mg/ml solution in saline). After 5 minutes, the dye was activated upon white light illumination (Leica, Spain, KL1500LCD) localized to the right hemisphere for 20 minutes.

We note here that the specifics of anesthesia, gender, mouse and stroke type are in line with previous stroke studies [32, 33]. Furthermore, in this work our goal was to demonstrate the application of the SCOT method, so extensive cortical lesions were used, and, therefore, a large region was illuminated to try to induce a strong perturbation. The aim of this study was not to answer any biological questions but to reconstruct the blood flow change and access the extent of the stroke in the animal to demonstrate the method.

2.4. SCOT data acquisition protocol

The animal was placed on a stereotaxic frame and prepared for the imaging as explained in Section 2.3. Before stroke induction, the animal was placed into the imaging setup as shown in Fig. 1. The SCOT scanning arm was then arranged to enable a multiple source scan on the mouse brain. The pixels were registered to spatial distances with a ruler imaged on the mouse skull. The ring was then filled with mineral oil. To ensure that the skull was contaminate free (no hair, bubbles, etc.), and that vessels were visible, green light (525 nm) images were acquired. This also allowed us to focus the camera and avoid the artifacts at this proof-of-concept stage. The green

light was turned off and a baseline measurement was collected as illustrated in Fig. 3. A stroke was then induced using the method explained in Section 2.3. After the white light illumination, 60 minutes was allowed for the Rose Bengal dye to clear from the brain prior to SCOT measurement. The system was refocused and mineral oil was reapplied before a second measurement was collected for the same scanning positions (Fig. 3). The MRI (see Section 2.2) data was collected 24 hours later. Animal was then sacrificed. In total nine animals (n=9) were measured.

2.5. Theory and algorithms

2.5.1. Pre-processing and data analysis

Raw data for both baseline and stroke were acquired as shown in Fig. 3. For each source position the center of mass was calculated. To ensure an accurate calculation, the images were thresholded to 50% of the maximum measured value. For visual evaluation and confirmation, the source positions were superimposed on the image of the mouse brain as shown in Fig. 2(a).

[Figure 3 about here.]

2.5.2. Reconstructing the relative cerebral blood flow

The statistics of the motion of the scatterers in the tissue (in our case dominated by red blood cells) impresses itself onto the fluctuations of the diffusely reflected speckle pattern at the surface of the tissue. In order to quantify the statistics of these fluctuations, SCOT calculates the square of speckle contrast, κ^2, defined as the ratio of variance (σ_I^2) to the square of the mean value (μ_I^2) of the intensity over time or over a small number of detectors, i.e., $\kappa^2 = \frac{\sigma_I^2}{\mu_I^2}$ [34].

The speckle contrast is furthermore related to the normalized electric field autocorrelation, $g_1(\mathbf{r}, \tau)$, [35] as follows:

$$\kappa^2(\mathbf{r}, T) = \frac{2\beta}{T} \int_0^T |g_1(\mathbf{r}, \tau)|^2 \left(1 - \frac{\tau}{T}\right) d\tau \ . \tag{1}$$

Here β is a constant, whose value depends on the detection optics as well as the different optical modes in the measurement, T is the exposure time of the detection system, τ is the correlation delay time and r is source-detector separation. The speckle contrast value (κ^2) varies between zero and one where higher values indicate slower fluctuations of the scatterers. Normalized electric field autocorrelation function (g_1) is related to the dynamics of the scattering medium which is described by the mean square displacement, $< \Delta r^2(r, \tau) >$, of the scatterers. It has been shown that the blood flow index (BFI) in tissues can be extracted using an effective Brownian motion coefficient (D_B) where $BFI = \alpha D_B \tau$ and α is the fraction of dynamic photon scattering events in medium [6, 36].

2.5.3. Noise correction of the speckle contrast

We have previously introduced a corrected speckle contrast, κ_c^2, [23] in order to account for the shot noise and dark noise variance associated with a digital camera sensor, defined as

$$\kappa_c^2(\mathbf{r}, T) = \frac{\sigma(I_c)^2 - \sigma_s^2 - \sigma_d^2}{\mu(I_c)^2} \tag{2}$$

where the corrected intensity (I_c) is $I_c = I - \mu_{I_d}$. Here I is the raw intensity image, μ_{I_d} and σ_d^2 are the mean intensity and the variance of the dark signals, respectively. The shot noise associated with the intensity images are accounted in the $\sigma_s^2 = \mu(I_c)$ term.

In SCOT, speckle contrast data is computed at several source-detector pairs obtained by scanning the sample along with an inversion model based on the first Born approximation [24, 37, 38], to get a three dimensional tomographic image of rCBF. A detailed description of SCOT and the derivation of all the steps can be found in Ref. [24]. The second part of the computational algorithm (forward problem) shown in Fig. 3 involves the computation of the speckle contrast from experimentally measured raw intensity images to speckle contrast with the noise correction (Eq.2).

2.5.4. Inversion algorithm and data analysis

To improve the SNR and to decrease computational load, the speckle contrast from four adjacent pixels were binned into a single pixel, Fig. 4. Computational grid was superimposed to the mouse brain as shown in Fig. 2(b), for visual confirmation of accuracy.

The baseline blood flow (BFI_B) was determined from an independent DCS measurement (source-detector separation of 4 mm). In the future, this can be done with a multi-exposure speckle imaging (MESI) measurement [17, 39] but due to single exposure time measurements of our present setup, current implementation of SCOT could not provide this information. The BFI from DCS was used to compute the Jacobian (J) as explained in Ref. [24]. From the computed Jacobian, ΔBFI was solved from $J \cdot \Delta BFI = \Delta\kappa^2$ here $\Delta\kappa^2$ is defined as $\kappa_{CS}^2 - \kappa_{CB}^2$ where κ_{CB} and κ_{CS} are corrected speckle contrast for baseline and stroke respectively. Appropriate regularization methods were employed as previously described in Refs. [24, 40].

2.6. Post processing

We found the maximum of blood flow change $|rCBF|$ in a region of interest (ROI) in the XZ plane (for the surface layer) manually. Then a "region growing" algorithm was used [41, 42] to identify all connected voxels that demonstrated an $|rCBF|$ change higher than 80% of the maximum rCBF change. From this thresholded volume of the three dimensional CBF images, a volume integral of relative cerebral blood flow was computed in a similar way as Refs. [24, 40].

The relative CBF (rCBF) is then defined as the ratio of the change in blood flow index (ΔBFI) to the baseline blood flow index (BFI_B):

$$rCBF(\%) = \frac{\Delta BFI}{BFI_B} \cdot 100[\%]. \tag{3}$$

The reconstructed and thresholded rCBF images are compared to the MRI data as follows. The SCOT and anatomical MRI images were registered to each other using the Bregma point. The optical data was then shifted and interpolated to coincide with the MRI co-ordinates and allow for a one-to-one comparison of the depth and breadth of the infarct. Since the computational grid used for SCOT is rectangular, the information about the curvature was used from the MRI to project the optical data onto the mouse brain for better visualization. The curvature correction is not used for the quantitative analysis.

3. Results

3.1. Pre-processing results: simulating laser speckle contrast imaging

Detectors that were less than 0.8 mm from the source position were excluded to avoid gross violations of the photon diffusion approximation. Fur-

thermore, detectors that were greater than 3 mm from the source were also excluded to avoid contamination by potential issues due to lower SNR. The corresponding detectors with the Born data, $\Delta\kappa^2$, for the specific sources (one, seven, ten and twenty) are shown in Fig. 4 for a representative animal. The source along the edge (source 1) of the image has a smaller number of detectors due to physical restrictions (dental cement, teflon ring, etc.). In comparison a source in the middle (source 8) of the image used all available detectors. The number of source-detector pairs varied between different animals; the minimum was 17336 and the maximum was 24613 with an average of 21182 over all nine animals, as described in Section 2.5.4. Each pixel consisted of the average of 2 by 2 pixels worth of speckle contrast which corresponds to a region of 11.2 by 11.2 μm and results in a high density scanning of the mouse brain.

[Figure 4 about here.]

The high-density nature of data allows us to construct images similar to traditional LSI by simply averaging the data from all valid source-detector positions. The resulting images for (a) baseline, (b) post-stroke, and, (c) perturbed ($\Delta\kappa^2$) speckle contrast are shown in Fig. 5. In comparison to the baseline (a), we see a higher speckle contrast (b) in the stroke region where photothrombosis was induced. This results in a large change in $\Delta\kappa^2$ as shown in panel (c). Once again, the high-density nature of the SCOT data can produce LSI-like images with a great deal of detail for near surface blood flow changes and the vasculature.

[Figure 5 about here.]

3.2. Inversion of the data and reconstruction of the images

A three dimensional grid with a total of 70400 voxels was used for the computation with X-Z plane of 64 x 55 voxels and 20 voxels into depth (Y) plane. After the suitable grid was placed, the next step was the reconstruction as described above.

The resulting reconstructed image of two different planes for a representative animal with a successful stroke is shown in Fig. 6(a). The top left image shows the superficial (X-Z) plane and we can see the CBF change due to the stroke. The maximum magnitude of $|rCBF|$ change was found and thresholded with the "region growing" algorithm. The top right panel, demonstrates the change in blood flow for each slice, with the lines passing through coordinates of the maximum relative blood flow change ($|rCBF|$) for both directions (X (dotted line) and Z (dashed line)). The bottom left panel in Fig. 6(a) shows the X-Y slice and the bottom right panel shows the calculated rCBF (%) through each slice in depth (Y (solid line)). To demonstrate the depth sensitivity of the SCOT, we also show the area of the infarct calculated by the MRI image in all slices as a bar plot (right y-axis). Both the magnitude of rCBF and infarct area measured by MRI show maximum change at the surface of the brain and decay with depth.

Fig. 6(b) demonstrates similar results from another animal where there was no detectable infarct despite an attempted photothrombosis. We see a small increase in rCBF in all directions possibly due to the brain reacting to the attempted photothrombosis. In the MRI images, after 24 hours, there was no detectable infarct area, hence there is no corresponding quantitative comparison with the MRI.

[Figure 6 about here.]

3.3. Magnetic resonance imaging and speckle contrast optical tomography comparison

One representative MRI image was selected and compared against the SCOT data, in Fig. 7. The Bregma position in the mouse brain was used to register the images, as explained in Section 2.6. In Fig. 7(a), we compare (left) the MRI image showing the infarct region in light gray (right) with a composite image of the overlaid, thresholded rCBF SCOT image and the MRI image (right) in (a) X-Y plane and (b) Y-Z plane. The reconstruction volume (the bigger block, red) that was used for SCOT reconstruction and the estimated maximum sensitivity volume (the smaller block, green) are also shown. The infarct volume measured at 24 hours and the thresholded rCBF image show remarkable agreement in different slices.

[Figure 7 about here.]

3.4. Summary for all nine animals

In Fig. 8(a), we show the norm of the Born data, $\Delta\kappa^2$, for all mice. Significant variations of the speckle contrast changes are observed between animals which will be reflected on the rCBF images.

Fig. 8(b) shows the corresponding rCBF quantified by the region-growing algorithm. The animals with a typical stroke (group: Stroke (MRI)) demonstrate a significant decrease in rCBF, while those without an observable infarct (group: No stroke (MRI)) have a moderate increase or no change. The stroke was confirmed visually from biopsies for the animals without MRI (no stroke (MRI)).

The extent of the stroke is quantified from the infarct volume measured by MRI and is plotted in Fig. 8(c) showing both the volume of the ipsilateral hemisphere and the infarct volume ("stroke"). In total, six animals were measured by MRI; three of them had a measurable infarct due to stroke (group: Stroke (MRI)) and three did not (group: No stroke (MRI)). As for the three animals that did not have a MRI (group: Stroke (no MRI)); one animal was omitted due to technical difficulties with the MRI but a typical infarct was visually observed on brain biopsy. Two animals (marked by (*)) did not survive the 24 hours but an extensive stroke was visually confirmed by brain biopsy. Extensive changes in both raw data (Fig. 8(a)) and reconstructed rCBF image (Fig. 8(b)) are in-line with the MRI findings (Fig. 8(c)).

[Figure 8 about here.]

4. Discussion

In vivo demonstration of SCOT was presented by imaging the mouse brain transcranially in a minimally invasive fashion – the scalp was retracted, but the skull was intact. Our SCOT implementation makes use of speckle contrast measurements obtained from high density source scanning imaged with a CCD camera resulting in thousands of source-detector pairs per animal. We have presented the pre-processing, tomographic inversion and post-processing details. Finally, we have induced a photothrombosis and compared the SCOT to the measured MRI anatomical images after 24 hours. The results indicate that SCOT is a viable method for imaging the small animal brain and quantifying the CBF changes in three dimensions. Furthermore, the high-density

SCOT data retains most of the information available to traditional LSI which makes it a versatile approach.

4.1. Speckle contrast optical tomography for high dense scanning and longitudinal imaging

To understand the benefits of SCOT, we compare the technology and the measured results to DCT which was previously employed on rats and mice. An early study combined DCT with DOT and measured CBF, cerebral blood volume, and blood oxygen saturation simultaneously [43]. Here twelve source positions were assigned in a 100 mm^2 area and measured by four fiber coupled detectors in a non-contact arrangement. In another application of DCT for longitudinal three dimensional tomography of rCBF during cortical spreading depression in a rat brain, three sources and eight detectors were arranged in an area of 72 mm^2 [22]. This study mapped the spread of the increased brain activity over time. Other applications included mapping the rodent leg for imaging bone grafts [44]. These studies have shown that DCT is a feasible approach but, as a low density measurement, suffered from poorer spatial resolution and potential artifacts in quantification.

DOT, on the other hand, was carried out both with fiber coupled individual detector arrays and with two-dimensional sensors such as different types of cameras [8]. The benefits of high-density scanning have been shown clearly in adults and in small animals [45, 46, 47, 48]. However, as mentioned before, direct information about CBF is not available from the intensity measurements used in traditional DOT.

We have presented high-density SCOT (Fig. 2 and Fig. 4) with a much greater number of measurements than DCT systems. Using a CCD camera

for detection, provides a flexible platform with several possible optimization strategies. For this feasibility study, we have used an average of 20 source positions in an area of 48 mm^2 and an average number of 21182 source-detector pairs. However, we have not used all pixels available as detectors but, rather, limited ourselves to keep to the photon diffusion regime and high SNR regions. Furthermore, we have combined four pixels to form a detector to achieve a better SNR. We note that the scanning system and the camera are well integrated and the setup is suitable for small animal imaging for longitudinal studies as shown in Fig. 1. One could readily speculate, given that SCOS in larger source-detector separations was demonstrated on the human arm [23], that the scalp can be kept intact with additional care to deal with any artifacts due to the superficial blood flow. Furthermore, this system could be extended to human measurements with an improved imaging system. This upgrade should allow for an effective and robust tissue interface (through appropriate optics) in a contact or a non-contact manner [49] as previously done with DOT and utilize higher sensitivity cameras with a larger dynamic range.

4.2. Information content of high-density SCOT

Although SCOT utilizes point source illumination, it is interesting to observe the cumulative effect of all the sources on the speckle contrast data as shown in Fig. 5. The results in this figure are a composite of different source-detector pairs for both the baseline and post-stroke induction images. The results shown in the figure can be compared to typical two dimensional topographic images obtained by LSI [12, 13] where depth information of blood flow is lacking. However, SCOT setup was able to obtain LSI-like resolution

while also retaining the depth information and is capable of a tomographic reconstruction of relative blood flow in small animals. We note that a multi-exposure approach was not employed in this study, but the current setup can be extended to such an approach with a loss of temporal resolution to achieve quantitative, absolute measurements of the baseline values as was done with LSI [17].

4.3. Quantification of the CBF and its extend by SCOT

Fig. 8(a) shows the change in speckle contrast due to the photothrombosis. A large range of values were observed. We have shown (Fig. 8(b)) that this was most likely due to the varying amount of damage induced by the photothrombosis. Two animals died before the necessary delay for the MRI imaging, 24 hours, due to what appeared to be an extensive stroke. No infarct was produced in three animals. Fig. 8(b) demonstrates the results from thresholded CBF changes with a region growing algorithm. Measured decrease in CBF (%) for animals with a typical infarct (n=4) was between 15 to 45 percent. A study of imaging photothrombotic ischemic stroke in freely moving rats using LSI reported a CBF (%) reduction of of 20-60% after 5 to 15 minutes of induction of stroke (see Fig. 2 in reference [50]). In another work [51], a 20-30% reduction in CBF was measured using LSI where cerebral venous ischemia was introduced in rats using the photothrombosis method.

It is a well known fact that diffuse optics based tomographic methods have an inherent tendency to reconstruct with a bias towards the scanning plane (planes near to source detector plane) which can be improved using a depth sensitive regularization [7]. An indirect measure of depth sensitivity of SCOT is demonstrated in Fig. 6(a) by plotting the mean value of the thresholded

value of rCBF change over X-Z plane as a function depth (along Y axis). A similar plot of the infarct area as a function of the depth is determined from the MRI images and plotted in in the same figure. Comparing CBF changes and the MRI infarct area in a slice, Fig. 6(a), one can reach a conclusion that the SCOT is indeed depth sensitive. Finally, the reconstructed images from the SCOT and corresponding MRI images are shown in Fig. 7. The extent of the reconstructed depth is evident from X-Y and Y-Z slices. MRI and corresponding SCOT images show a qualitative agreement.

Different localized changes, more complex reconstruction algorithms (e.g. a non-linear, iterative approach) and a careful phantom study would, in the future, help us quantify these parameters with more accuracy. However, this is beyond the scope of this work.

4.4. Drawbacks and further improvements

There is room for improvement in several aspects of the SCOT system and measurement protocol. The current system is limited by a combination of the scanner opto-mechanics and the camera. Faster scanning opto-mechanics and a faster frame rate camera would remedy these limitations. Both are readily available, albeit with a higher cost. We have used a single exposure time which limited our ability to fit the baseline blood flow values. This can be remedied with a multi-exposure time system and is readily possible with the current camera. However, we opted not to implement it due to the relatively slow frame rate of this camera. Furthermore, we have used *a priori* estimates of the optical properties (absorption coefficient of 0.15 cm^{-1}, reduced scattering coefficient 15 cm^{-1}) from the literature. This can be partially remedied by utilizing the source-detector distance dependence of the

detected mean-intensity at high exposure times (blurring out the speckles) to extract the effective attenuation coefficient or by developing a full hybrid system with a multi-wavelength NIRS-DOS as was done with previous DCT work [43]. We note that it was previously shown that large relative changes in CBF measured by DCS are minimally affected by these parameters [52] so our results are expected to be accurate.

Large perturbations in the speckle contrast were observed, in particular in animals (group: Stroke (no MRI)*), and are problematic for the first order Born approximation that we have employed [24]. However, more advanced non-linear, iterative methods can be adapted to SCOT despite the added complexity of the speckle contrast formalism [24]. The present reconstruction algorithm assumes a homogeneous background medium which can be improved by adopting a finite element based forward solver for the correlation diffusion equation (CDE) [53]. An anatomical MRI image of the particular animal or a mouse brain atlas can be used as the starting point. Furthermore, regions of high absorption (e.g. over large blood vessels) and short source-detector separations may be problematic for the correlation diffusion model. A more advanced model based on Monte Carlo or higher order approximations of the correlation diffusion model [54] would provide a more accurate estimate of light transport in tissue. In fact, the LSI-like high resolution information that is available from SCOT can allow us to, at least, introduce heterogeneities as priors to the upper layers where it matters the most.

5. Conclusion

We have presented *in vivo* measurements with speckle contrast optical tomography (SCOT). High-density SCOT was employed on the mouse brain and evaluated the depth-resolved changes in cerebral blood flow (CBF) due to photothrombosis-induced ischemic stroke. These results pave the way for developing high-density SCOT as a tool for studying CBF in small animal models in a non-invasive, longitudinal and quantitative manner.

6. Acknowledgements

The project was funded by Fundació CELLEX Barcelona, Ministerio de Economía y Competitividad (PHOTODEMENTIA (DPI2015-64358-c1 and c2 MINECO/FEDER), the "Severo Ochoa" Programme for Centres of Excellence in R&D (SEV-2015-0522), the Obra social "la Caixa" Foundation (LlumMedBcn). J.L.Hollmann acknowledges the Marie Curie COFUND (FP7-PEOPLE-2013-COFUND) fellowship. We acknowledge useful discussions with Dr Ernesto Vidal Rosas.

References

[1] Alois Zauner and J Paul Muizelaar. Brain metabolism and cerebral blood flow. *Head injury*, pages 89–99, 1997.

[2] Max Wintermark, Nancy J Fischbein, Wade S Smith, Nerissa U Ko, Marcel Quist, and William P Dillon. Accuracy of dynamic perfusion ct with deconvolution in detecting acute hemispheric stroke. *American journal of neuroradiology*, 26(1):104–112, 2005.

[3] Marc Fisher and Gregory W Albers. Applications of diffusion–perfusion magnetic resonance imaging in acute ischemic stroke. *Neurology*, 52(9):1750–1750, 1999.

[4] Josef Vymazal, Aaron M Rulseh, Jiří Keller, and Ladislava Janouskova. Comparison of ct and mr imaging in ischemic stroke. *Insights into imaging*, 3(6):619–627, 2012.

[5] Anna Devor, Sava Sakadžić, Vivek J Srinivasan, Mohammad A Yaseen, Krystal Nizar, Payam A Saisan, Peifang Tian, Anders M Dale, Sergei A Vinogradov, Maria Angela Franceschini, et al. Frontiers in optical imaging of cerebral blood flow and metabolism. *Journal of Cerebral Blood Flow & Metabolism*, 32(7):1259–1276, 2012.

[6] Turgut Durduran, Regine Choe, WB Baker, and Arjun G Yodh. Diffuse optics for tissue monitoring and tomography. *Reports on Progress in Physics*, 73(7):076701, 2010.

[7] Joseph P Culver, Andrew M Siegel, Jonathan J Stott, and David A Boas. Volumetric diffuse optical tomography of brain activity. *Optics letters*, 28(21):2061–2063, 2003.

[8] Zi-Jing Lin, Ming Ren, Lin Li, Yueming Liu, Jianzhong Su, Shao-Hua Yang, and Hanli Liu. Interleaved imaging of cerebral hemodynamics and blood flow index to monitor ischemic stroke and treatment in rat by volumetric diffuse optical tomography. *Neuroimage*, 85:566–582, 2014.

[9] Zi-Jing Lin, Haijing Niu, Yueming Liu, Jianzhong Su, and Hanli Liu. Ccd-camera-based diffuse optical tomography to study ischemic stroke

in preclinical rat models. In *Proc. of SPIE Vol*, volume 7896, pages 78960R–1, 2011.

[10] Zi-Jing Lin, Haijing Niu, Lin Li, and Hanli Liu. Volumetric diffuse optical tomography for small animals using a ccd-camera-based imaging system. *International Journal of Optics*, 2012, 2012.

[11] Brian R White and Joseph P Culver. Quantitative evaluation of high-density diffuse optical tomography: in vivo resolution and mapping performance. *Journal of biomedical optics*, 15(2):026006–026006, 2010.

[12] Andrew K Dunn. Laser speckle contrast imaging of cerebral blood flow. *Annals of biomedical engineering*, 40(2):367–377, 2012.

[13] David A Boas and Andrew K Dunn. Laser speckle contrast imaging in biomedical optics. *Journal of biomedical optics*, 15(1):011109–011109, 2010.

[14] Andrew K Dunn, Hayrunnisa Bolay, Michael A Moskowitz, and David A Boas. Dynamic imaging of cerebral blood flow using laser speckle. *Journal of Cerebral Blood Flow & Metabolism*, 21(3):195–201, 2001.

[15] Ulrich Dirnagl, Bruce Kaplan, Michael Jacewicz, and William Pulsinelli. Continuous measurement of cerebral cortical blood flow by laser-doppler flowmetry in a rat stroke model. *Journal of Cerebral Blood Flow & Metabolism*, 9(5):589–596, 1989.

[16] Henning Piilgaard and Martin Lauritzen. Persistent increase in oxygen consumption and impaired neurovascular coupling after spreading de-

pression in rat neocortex. *Journal of Cerebral Blood Flow & Metabolism*, 29(9):1517–1527, 2009.

[17] Ashwin B Parthasarathy, SM Shams Kazmi, and Andrew K Dunn. Quantitative imaging of ischemic stroke through thinned skull in mice with multi exposure speckle imaging. *Biomedical optics express*, 1(1):246–259, 2010.

[18] David A Boas, LE Campbell, and Arjun G Yodh. Scattering and imaging with diffusing temporal field correlations. *Physical review letters*, 75(9):1855, 1995.

[19] DA Boas, MA O'leary, B Chance, and AG Yodh. Scattering of diffuse photon density waves by spherical inhomogeneities within turbid media: analytic solution and applications. *Proceedings of the National Academy of Sciences*, 91(11):4887–4891, 1994.

[20] Rickson C Mesquita, Turgut Durduran, Guoqiang Yu, Erin M Buckley, Meeri N Kim, Chao Zhou, Regine Choe, Ulas Sunar, and Arjun G Yodh. Direct measurement of tissue blood flow and metabolism with diffuse optics. *Philosophical Transactions of the Royal Society of London A: Mathematical, Physical and Engineering Sciences*, 369(1955):4390–4406, 2011.

[21] Cecil Cheung, Joseph P Culver, Kasushi Takahashi, Joel H Greenberg, and AG Yodh. In vivo cerebrovascular measurement combining diffuse near-infrared absorption and correlation spectroscopies. *Physics in medicine and biology*, 46(8):2053, 2001.

[22] Chao Zhou, Guoqiang Yu, Daisuke Furuya, Joel Greenberg, Arjun Yodh, and Turgut Durduran. Diffuse optical correlation tomography of cerebral blood flow during cortical spreading depression in rat brain. *Optics express*, 14(3):1125–1144, 2006.

[23] Claudia P Valdes, Hari M Varma, Anna K Kristoffersen, Tanja Dragojevic, Joseph P Culver, and Turgut Durduran. Speckle contrast optical spectroscopy, a non-invasive, diffuse optical method for measuring microvascular blood flow in tissue. *Biomedical optics express*, 5(8):2769–2784, 2014.

[24] Hari M Varma, Claudia P Valdes, Anna K Kristoffersen, Joseph P Culver, and Turgut Durduran. Speckle contrast optical tomography: A new method for deep tissue three-dimensional tomography of blood flow. *Biomedical optics express*, 5(4):1275–1289, 2014.

[25] Renzhe Bi, Jing Dong, Chueh Loo Poh, and Kijoon Lee. Optical methods for blood perfusion measurement theoretical comparison among four different modalities. *JOSA A*, 32(5):860–866, 2015.

[26] Renzhe Bi, Jing Dong, and Kijoon Lee. Deep tissue flowmetry based on diffuse speckle contrast analysis. *Optics letters*, 38(9):1401–1403, 2013.

[27] Renzhe Bi, Jing Dong, and Kijoon Lee. Multi-channel deep tissue flowmetry based on temporal diffuse speckle contrast analysis. *Optics express*, 21(19):22854–22861, 2013.

[28] Chong Huang, Daniel Irwin, Yu Lin, Yu Shang, Lian He, Weikai Kong, Jia Luo, and Guoqiang Yu. Speckle contrast diffuse correlation tomogra-

phy of complex turbid medium flow. *Medical physics*, 42(7):4000–4006, 2015.

[29] Chong Huang, Myeongsu Seong, Joshua Paul Morgan, Siavash Mazdeyasna, Jae Gwan Kim, Jeffrey Todd Hastings, and Guoqiang Yu. Low-cost compact diffuse speckle contrast flowmeter using small laser diode and bare charge-coupled-device. *Journal of Biomedical Optics*, 21(8):080501–080501, 2016.

[30] Cheng Qian, Pei-Cheng Li, Yun Jiao, Hong-Hong Yao, Yu-Chen Chen, Jian Yang, Jie Ding, Xiang-Yu Yang, and Gao-Jun Teng. Precise characterization of the penumbra revealed by mri: A modified photothrombotic stroke model study. *PloS one*, 11(4):e0153756, 2016.

[31] Xavier de la Rosa, Alvaro Cervera, Anna K Kristoffersen, Claudia P Valdés, Hari M Varma, Carles Justicia, Turgut Durduran, Ángel Chamorro, and Anna M Planas. Mannose-binding lectin promotes local microvascular thrombosis after transient brain ischemia in mice. *Stroke*, 45(5):1453–1459, 2014.

[32] Jung-Kil Lee, Min-Sung Park, Yeon-Seong Kim, Kyung-Sub Moon, Sung-Pil Joo, Tae-Sun Kim, Jae-Hyoo Kim, and Soo-Han Kim. Photochemically induced cerebral ischemia in a mouse model. *Surgical neurology*, 67(6):620–625, 2007.

[33] Lucie A Low, Lucy C Bauer, and Brenda A Klaunberg. Comparing the effects of isoflurane and alpha chloralose upon mouse physiology. *PloS one*, 11(5):e0154936, 2016.

[34] J David Briers. Laser doppler, speckle and related techniques for blood perfusion mapping and imaging. *Physiological measurement*, 22(4):R35, 2001.

[35] Ranjini Bandyopadhyay, AS Gittings, SS Suh, PK Dixon, and DJ Durian. Speckle-visibility spectroscopy: A tool to study time-varying dynamics. *Review of Scientific Instruments*, 76(9):093110, 2005.

[36] David A Boas, Sava Sakadžić, Juliette Selb, Parisa Farzam, Maria Angela Franceschini, and Stefan A Carp. Establishing the diffuse correlation spectroscopy signal relationship with blood flow. *Neurophotonics*, 3(3):031412–031412, 2016.

[37] Simon R Arridge and John C Schotland. Optical tomography: forward and inverse problems. *Inverse Problems*, 25(12):123010, 2009.

[38] MCW van van Rossum and Th M Nieuwenhuizen. Multiple scattering of classical waves: microscopy, mesoscopy, and diffusion. *Reviews of Modern Physics*, 71(1):313, 1999.

[39] Ashwin B Parthasarathy, Erica L Weber, Lisa M Richards, Douglas J Fox, and Andrew K Dunn. Laser speckle contrast imaging of cerebral blood flow in humans during neurosurgery: a pilot clinical study. *Journal of biomedical optics*, 15(6):066030–066030, 2010.

[40] Brian Richard White. *Developing high-density diffuse optical tomography for neuroimaging*. 2012.

[41] Steven W Zucker. Region growing: Childhood and adolescence. *Computer graphics and image processing*, 5(3):382–399, 1976.

[42] Regine Choe, Soren D Konecky, Alper Corlu, Kijoon Lee, Turgut Durduran, David R Busch, Saurav Pathak, Brian J Czerniecki, Julia Tchou, Douglas L Fraker, et al. Differentiation of benign and malignant breast tumors by in-vivo three-dimensional parallel-plate diffuse optical tomography. *Journal of biomedical optics*, 14(2):024020–024020, 2009.

[43] Joseph P Culver, Turgut Durduran, Daisuke Furuya, Cecil Cheung, Joel H Greenberg, and AG Yodh. Diffuse optical tomography of cerebral blood flow, oxygenation, and metabolism in rat during focal ischemia. *Journal of cerebral blood flow & metabolism*, 23(8):911–924, 2003.

[44] Songfeng Han, Ashley R Proctor, Joseph B Vella, Danielle SW Benoit, and Regine Choe. Non-invasive diffuse correlation tomography reveals spatial and temporal blood flow differences in murine bone grafting approaches. *Biomedical Optics Express*, 7(9):3262–3279, 2016.

[45] Adam T Eggebrecht, Brian R White, Silvina L Ferradal, Chunxiao Chen, Yuxuan Zhan, Abraham Z Snyder, Hamid Dehghani, and Joseph P Culver. A quantitative spatial comparison of high-density diffuse optical tomography and fmri cortical mapping. *Neuroimage*, 61(4):1120–1128, 2012.

[46] Adam T Eggebrecht, Silvina L Ferradal, Amy Robichaux-Viehoever, Mahlega S Hassanpour, Hamid Dehghani, Abraham Z Snyder, Tamara Hershey, and Joseph P Culver. Mapping distributed brain function and networks with diffuse optical tomography. *Nature photonics*, 8(6):448, 2014.

[47] Benjamin W Zeff, Brian R White, Hamid Dehghani, Bradley L Schlaggar, and Joseph P Culver. Retinotopic mapping of adult human visual cortex with high-density diffuse optical tomography. *Proceedings of the National Academy of Sciences*, 104(29):12169–12174, 2007.

[48] Hamid Dehghani, Brian R White, Benjamin W Zeff, Andrew Tizzard, and Joseph P Culver. Depth sensitivity and image reconstruction analysis of dense imaging arrays for mapping brain function with diffuse optical tomography. *Applied optics*, 48(10):D137–D143, 2009.

[49] M Mazurenka, L Di Sieno, G Boso, D Contini, A Pifferi, A Dalla Mora, A Tosi, H Wabnitz, and R Macdonald. Non-contact in vivo diffuse optical imaging using a time-gated scanning system. *Biomedical optics express*, 4(10):2257–2268, 2013.

[50] Hongyang Lu, Yao Li, Lu Yuan, Hangdao Li, Xiaodan Lu, and Shanbao Tong. Induction and imaging of photothrombotic stroke in conscious and freely moving rats. *Journal of biomedical optics*, 19(9):096013–096013, 2014.

[51] Yasuhiro Takeshima, Hitoshi Miyake, Ichiro Nakagawa, Yasushi Motoyama, Young-Su Park, and Hiroyuki Nakase. Visualization of regional cerebral blood flow dynamics during cortical venous occlusion using laser speckle contrast imaging in a rat model. *Journal of Stroke and Cerebrovascular Diseases*, 24(10):2200–2206, 2015.

[52] Wesley B Baker, Ashwin B Parthasarathy, David R Busch, Rickson C

Mesquita, Joel H Greenberg, and AG Yodh. Modified beer-lambert law for blood flow. *Biomedical optics express*, 5(11):4053–4075, 2014.

[53] Hari M Varma, AK Nandakumaran, and RM Vasu. Study of turbid media with light: Recovery of mechanical and optical properties from boundary measurement of intensity autocorrelation of light. *JOSA A*, 26(6):1472–1483, 2009.

[54] Maureen A O'Leary. *Imaging with diffuse photon density waves*. PhD thesis, University of Pennsylvania, 1996.

List of Figures

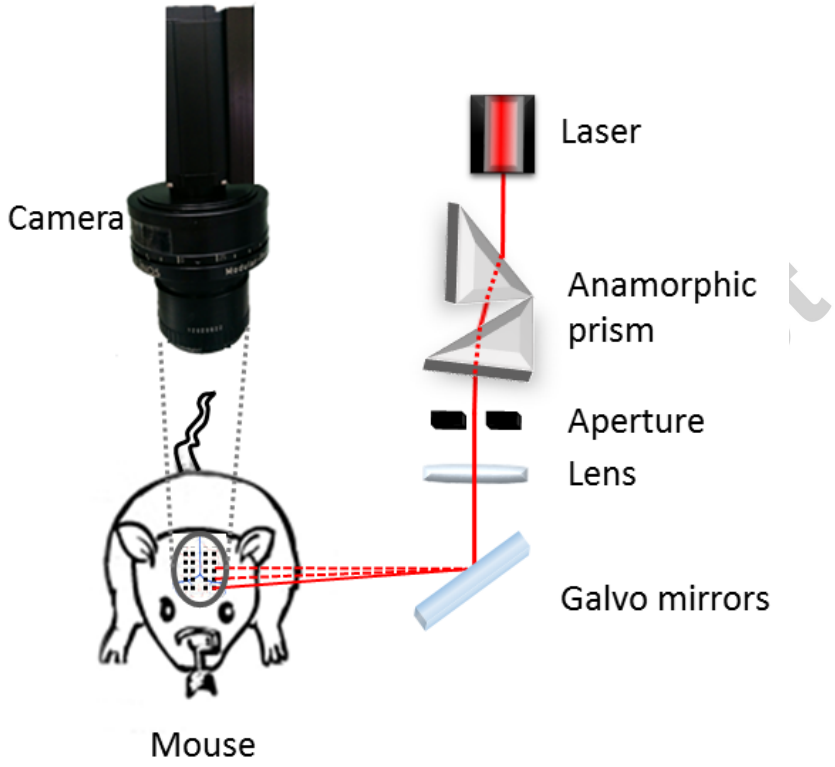

Figure 1: An illustration of the scanning system consisting of the laser, the anamorphic prism, the aperture, the lens and the galvo-mirrors, the camera and the animal on a stereotaxic frame. Mouse drawing courtesy of Yookyung Choe.

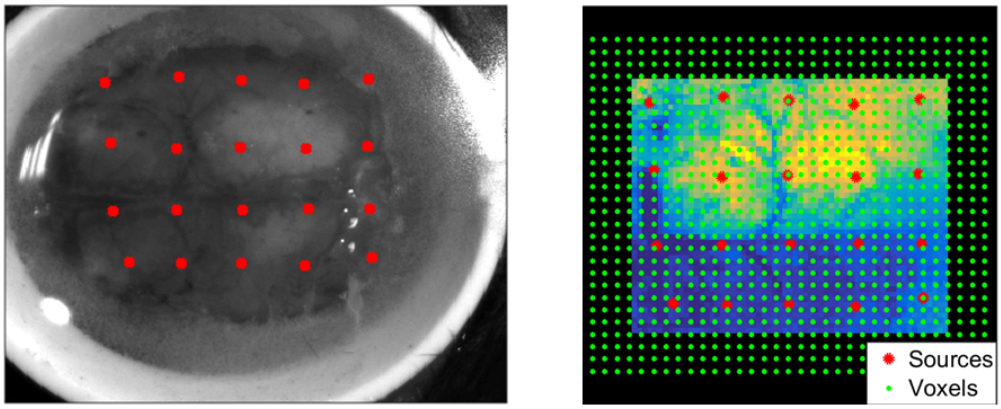

Figure 2: (a) A photo of the mouse head showing the cleared skull, the ring for containing the liquids and the placement of the sources (red dot). (b) A sample data set showing the placement of the sources (red larger dots) and the voxel positions (green smaller dots) that are used for the inversion.

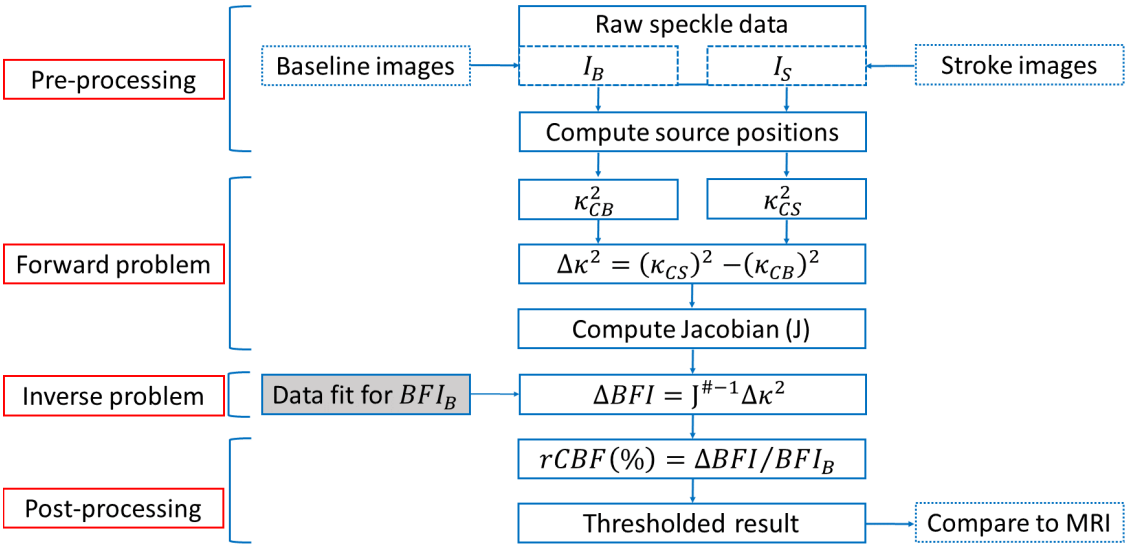

Figure 3: A flow-chart representing the pre- and post-processing algorithms for the SCOT reconstruction.

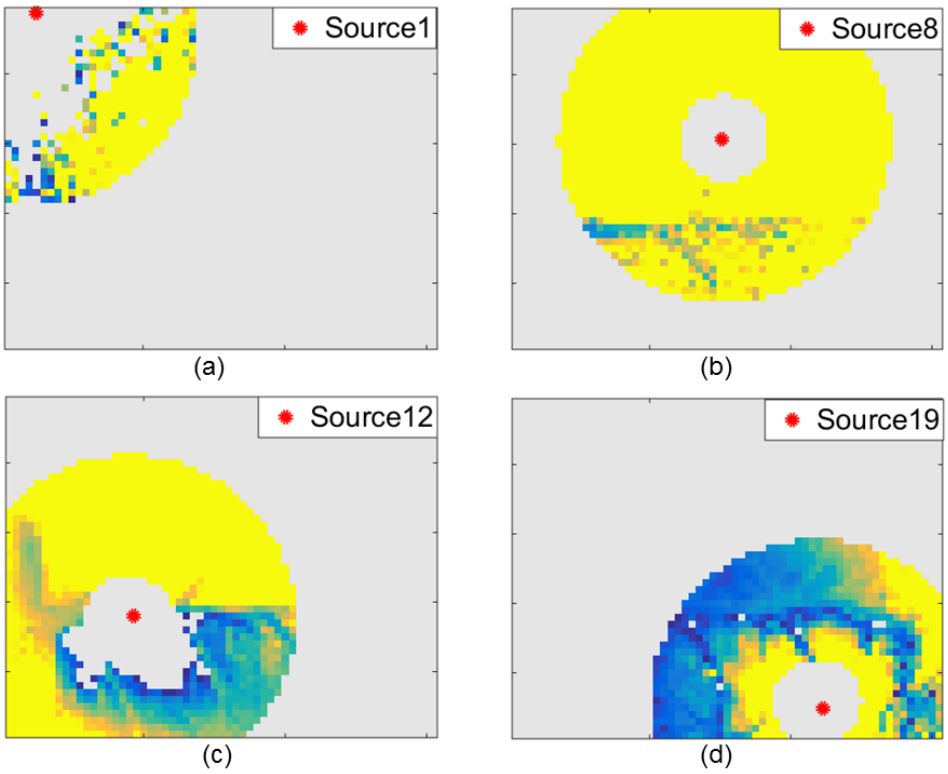

Figure 4: Sample representations of the detectors that are used for source positions 1, 8, 12 and 19 where the detectors that are utilized are those in the range of 0.8-3 mm around the source. The corresponding data is shown in false-color and light areas indicate regions that are not utilized. The detectors are presented from calculated Born data.

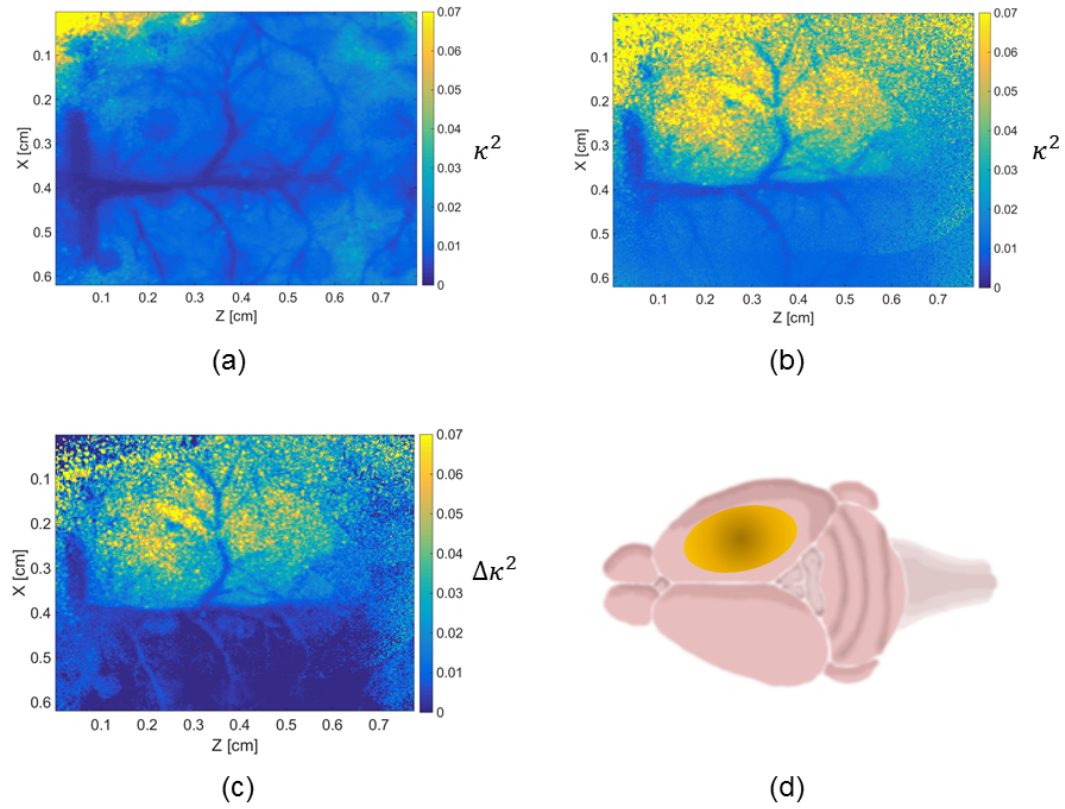

Figure 5: Laser speckle contrast images from a representative animal where panel (a) shows the laser speckle image before the stroke induction (baseline), (b) after the stroke is induced and (c) the difference between LSI images, (d) illustrates the mouse brain with the stroke in the right hemisphere.

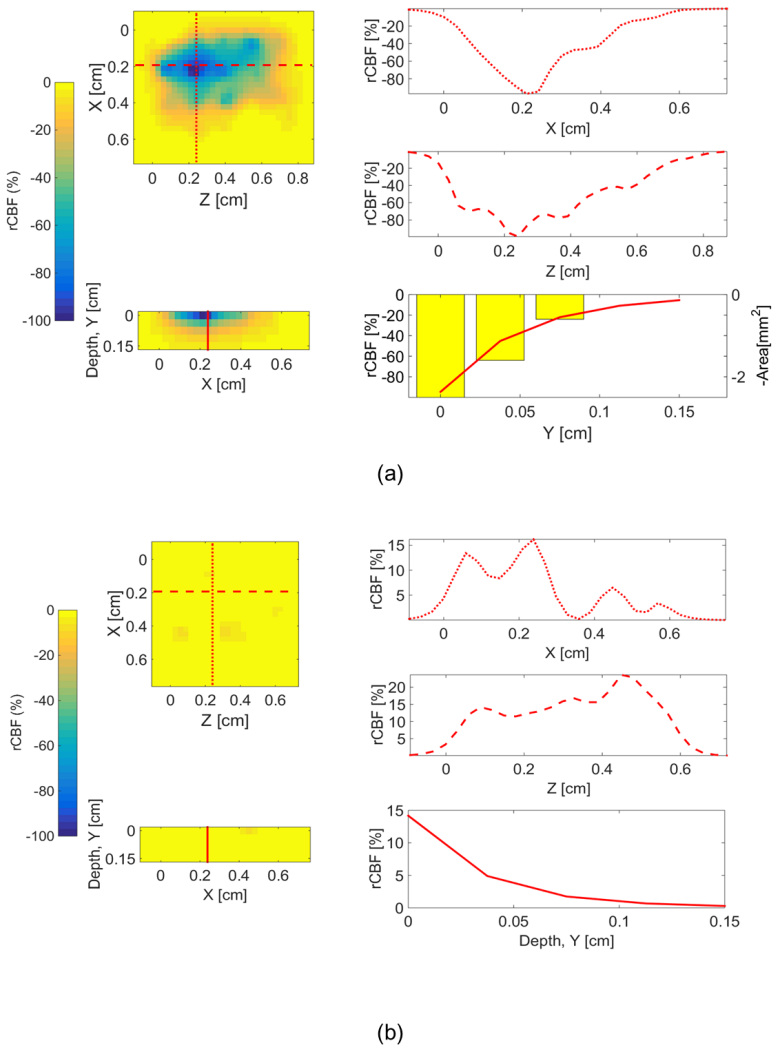

Figure 6: The results from two representative animals are shown for (a) an animal with a infarct and (b) an animal that did not have an infarct or edema after photothrombosis. The reconstructed image is shown in two slices (left column); the superficial (X-Z) plane and a slice through depth (X-Y). The corresponding changes in rCBF for all three axis are shown in the right column. In the transverse axis, we also indicate, how the infarct area (assessed by MRI at 24 hours) decreases with depth (bar plot, right y-axis) for the animal with a measurable infarct (a).

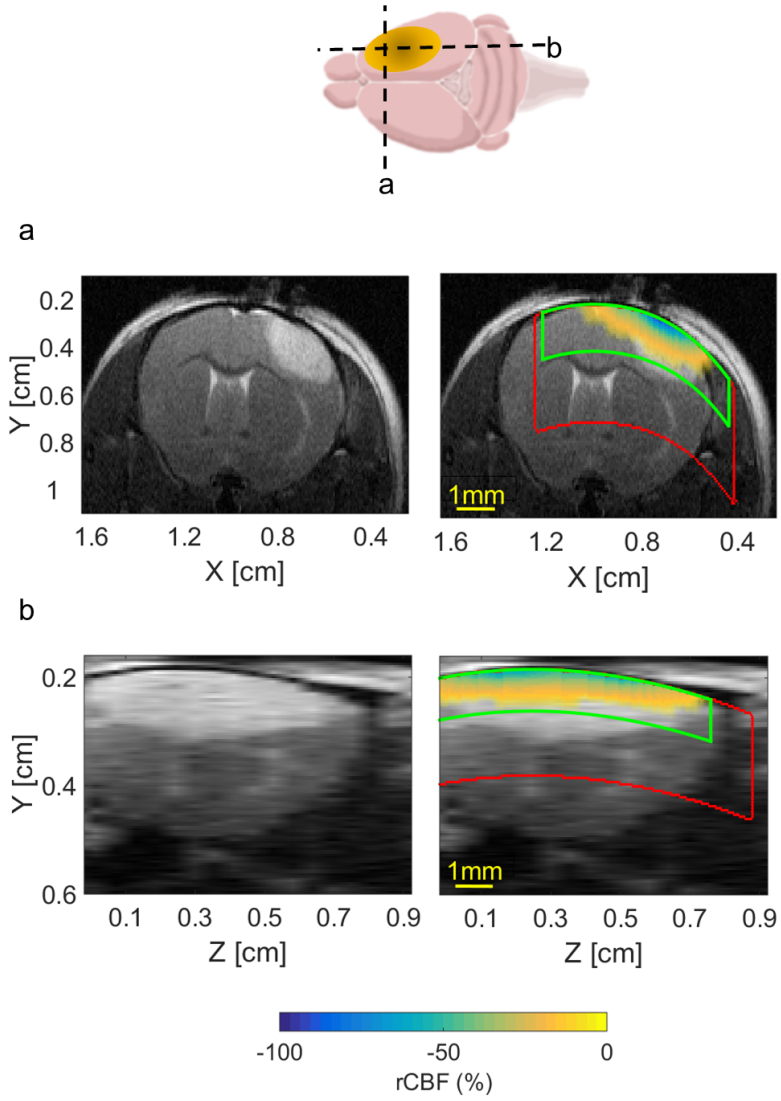

Figure 7: Comparison of the MRI data with the reconstructed and thresholded SCOT data is shown for a representative animal used in the previous figures. In panels (a) and (b), the left column, the MRI slices are shown. The lighter volume on the right hemisphere corresponds to the infarct induced by photothrombosis. In panels (a) and (b), the right column, the corresponding thresholded SCOT image is overlaid onto the MRI image. The region outlined by green illustrates the true sensitivity of SCOT whereas the red region illustrates the reconstruction grid.

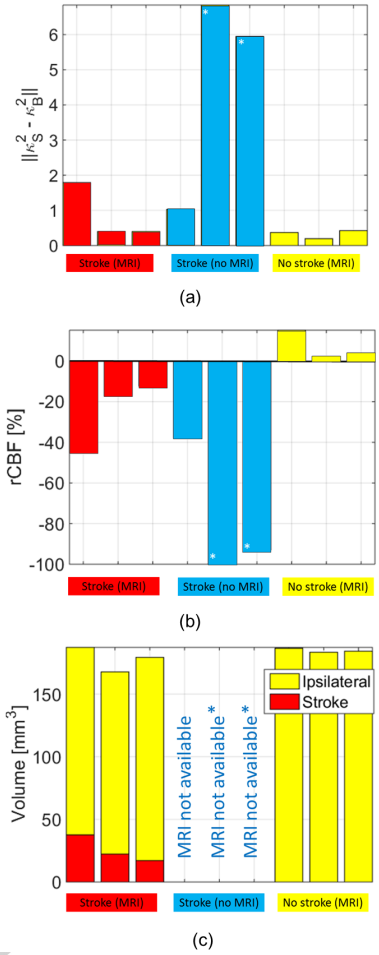

Figure 8: For all nine mice, Born of data, $\Delta\kappa^2$ is shown in (a). In panel (b), the extracted regional CBF from all animals is shown. It is clear that all animals with a significant percent of the hemisphere affected by the stroke confirmed by MRI (n=3) or visually (n=3) showed a decrease in CBF. Three animals without a detectable infarct showed a minimal change in CBF (or a small increase) The infarct volume ("stroke", red bars) and the full ipsilateral hemisphere volume (yellow bars) from MRI is shown in panel (c). In total, six animals were measured by MRI; three of them had a measurable infarct due to stroke (group: Stroke(MRI)) and three did not (group: No stroke (MRI)). For the three animals that did not have MRI (group: Stroke (no MRI)), two animals (marked by (*)) did not survive the 24 hours and a massive stroke was visually confirmed by brain biopsy. MRI is not available for first animal in stroke (no MRI) group due to technical reasons. A typical infarct was visually observed on brain biopsy.